frontiers | Frontiers in Marine Science

TYPE Original Research
PUBLISHED 01 March 2023
DOI 10.3389/fmars.2023.1143925

OPEN ACCESS

EDITED BY
Yi Pan,
Hohai University, China

REVIEWED BY
Yupeng Ren,
Ocean University of China, China
Chunyang Xu,
Hohai University, China

*CORRESPONDENCE
Zhe Huang
huangzhe1829@tju.edu.cn
Yuchuan Bai
ychbai@tju.edu.cn

SPECIALTY SECTION
This article was submitted to Coastal Ocean Processes, a section of the journal Frontiers in Marine Science

RECEIVED 13 January 2023
ACCEPTED 01 February 2023
PUBLISHED 01 March 2023

CITATION
Wang G, Feng X, Zhang J, Huang Z, Bai Y, Song W and Xu H (2023) A numerical study on the responses of coastal water quality to river runoff after heavy rainfall in the case of a complex coastline with two artificial islands.
Front. Mar. Sci. 10:1143925.
doi: 10.3389/fmars.2023.1143925

A numerical study on the responses of coastal water quality to river runoff after heavy rainfall in the case of a complex coastline with two artificial islands

Gang Wang[1,2,3], Xin Feng[2,3], Jiabo Zhang[2,3], Zhe Huang[1,3]*, Yuchuan Bai[1,3]*, Wei Song[4] and Haijue Xu[1]

[1]State Key Laboratory of Hydraulic Engineering Simulation and Safety, Tianjin University, Tianjin, China, [2]The Eighth Geological Brigade of Hebei Bureau of Geology and Mineral Resources Exploration, Qinhuangdao, China, [3]Marine Ecological Restoration and Smart Ocean Engineering Research Center of Hebei Province, Qinhuangdao, China, [4]Key Laboratory of Marine Eco-Environmental Science and Technology, First Institute of Oceanography, Ministry of Natural Resources, Qingdao, China

Heavy rainfall causes large volumes of freshwater and nutrient salts to flow from rivers into the sea. This leads to major changes in the ecological environment of estuarine waters in a short period of time. The responses of the estuarine hydro-environment become more complex with the concentrated construction of artificial structures, which is a major cause of marine ecological disasters. This paper considers the Tang Estuary in Qinhuangdao, where artificial structures (e.g., ports, artificial islands, and bridges) are concentrated, as a prototype with the weak tidal dynamic environment. A nested prototype of hydrodynamics and water quality was established using a Delft3D model, with coupled waves and flows. The model was used to simulate the spatial and ephemeral characteristics of the short-term responses of ecological environmental factors, such as dissolved inorganic nitrogen (DIN), nitrate-nitrogen (i.e., NO_3-N), ammonium-nitrogen (NH_4-N), and orthophosphate (i.e., PO_4-P), to an episode of heavy rainfall in August 2022. The results showed that concentrations of DIN and NO_3-N in the source areas remain high after the flooding process. The concentration recovered to normal values approximately 5.5 days after the flooding process. In contrast, NH_4-N and PO_4-P showed a response with ephemeral correspondence with the flooding process, and concentration recovery took only approximately 1 day. This paper proposes two short-term response modes of pollutant diffusion, which provide help in exploring the role of hydro-environmental changes in offshore algal hazards and the effect of permeable buildings on pollutant dispersion. This additionally provides possibilities with the forecasting of red tide and green tide, and for their prevention in the future.

KEYWORDS

heavy rainfall, river runoff, coastal water quality, land-based pollutants, artificial islands

1 Introduction

The Bohai Sea accounts for only 1.6% of China's national sea area but receives 32.2% of the country's pollutants (Zhang et al., 2006). Monitoring data show that land input dominates in terms of the sources of marine pollutants in the Bohai Sea, accounting for more than 80% of pollution, and 95% of these land-based pollutants are discharged from several estuaries (Zhao and Kong, 2000; Liu, 2010; Luan et al., 2016; Liu et al., 2017). Affected by monsoon and human activities, it is not obvious how pollutants are concentrated to discharge into the Bohai Sea along with land stream at the wet season, even in several short flood discharge processes with heavy rainfall. This land-based pollution leads to seawater eutrophication, which can increase the chances of ecological disasters in ecologically sensitive areas, such as red tides and green tides in the inner bay and coastlines near urban areas (Fletcher, 1996; Lappalainen and Ponni, 2000; Han et al., 2003; Pedersen and Borum, 2010). They may also cause jellyfish blooms as a result of estuarine eutrophication and an increase in small zooplankton and artificial structures (Lucas et al., 2012; Riisgard and Hoffmann, 2012; Makabe et al., 2014; Gu et al., 2017).

Qinhuangdao is located on the west coast of the Bohai Bay at an M2 amphidromic point in the open sea, with a small tidal range and weak tidal current. Affected by intense human activities, its coastline utilization patterns are diversely distributed. Ports, aquaculture, sand beaches, artificial islands, and primitive tidal flats are alternately distributed along the coastline. In recent years, its coastal waters have been more significantly affected by river pollutants flowing into the sea and have been seriously threatened by ecological disasters such as red tide, green tide, and jellyfish blooms. In particular, more attention should be paid to the Golden Dream Bay area, because this is located in the middle of the coastline of Qinhuangdao and its capacity for water exchange and pollutant transport is weakened by structures such as artificial islands, docks, and bridges (Kuang et al., 2015; Pan et al., 2018; Kuang et al., 2019; Pan et al., 2020; Kuang et al., 2021; Pan et al., 2022). Divided by the prismatic island in the estuary, a large amount of flood discharge sediment enters the Golden Dream Bay (Sheng et al., 2016). According to monitoring data, there were 43 red tide disasters in the Qinhuangdao sea area between 2001 and 2014 (Zhai et al., 2016), and 24 red tide disasters between 2015 and 2022. The occurrence of red tide disasters led to the deterioration of the water environment and damaged the aquaculture. Some toxic red tides even seriously threatened human lives and property. For example, the brown tide caused by *Aureococcus anophagefferens* began to appear in 2009 and occurred every year until 2014. During the period of the brown tide, the concentration of dissolved organic nitrogen (DON) was more than five times that of dissolved inorganic nitrogen (DIN) (Zhou et al., 2023). A higher DON concentration and lower levels of inorganic nutrients are suitable conditions for the growth of brown tide algae, whereas lower DIN limits the growth of brown tide algae (Zhang QC. et al., 2020). Another example is the seafood poisoning incident in 2016. This was mainly caused by the toxic species *Alexandrium catenella* (Yu et al., 2021; Tang et al., 2022a). Surficial sediments sampled in the area showed a decreasing trend from northeast to southwest (Tang et al,. 2022b). These ecological disasters are closely related to the levels of nitrogen (N) and phosphorus (P) in the water (Conley, 2000). These elements mainly come from river discharge, especially during periods of extreme rainfall, when the flow of rivers into the sea increases sharply (Meybeck, 1982).

Since 2015, large-scale algal blooms have occurred in the coastal area of Qinhuangdao Golden Dream Bay from April to September every year. The green tide in Qinhuangdao is of local origin and has different origins and development patterns than that of the Yellow Sea (Han et al., 2019). It has a significant positive correlation with the biomass of attached and floating *Pistia stratiotes*. The concentration of nitrate-nitrogen (i.e., NO_3-N) is the most important factor affecting the abundance of micro-propagules (Han et al., 2022). As a starting point, it is proposed that the outbreak of green tide in this area may be related to the eutrophication of estuarine waters and the weakening of regional hydrodynamics caused by the construction of artificial islands (Song et al., 2019). Research on the combination of green tide algae and micro- and nano-phytoplankton suggests that dissolved organic nitrogen (DON) and dissolved organic phosphorus (DOP) will promote biodiversity and the growth of micro- and nano-phytoplankton, and that low levels of dissolved inorganic phosphorus (DIP) will inhibit growth. In a sea environment with a suitable temperature and high concentrations of dissolved organic nitrogen (DON) and N/P, the outbreak of green tide algae will accelerate the transformation of the micro- and nano-phytoplankton community from dominant diatom species to dominant dinoflagellate species (Zhang et al., 2022).

Although there have been some studies conducted on the sea area near the Tang Estuary, a main entrance of drained river flow affecting the Golden Dream Bay, these have focused on the hydrodynamic effect of a single artificial island or an artificial island group. Researchers have not studied the hydrodynamics and pollutant diffusion in the sea area under the influence of the full set of relevant conditions (consisting of the artificial island group, wharf, island bridge, and coastal bathing beach) during flood water flow, which is often the key factor leading to a high degree of short-term eutrophication and short-term outbreaks of ecological disasters in the sea area. Considering the influence of diverse human activities, such as the construction of artificial islands and island bridges, Delft3D was adopted to establish a wave–current coupling hydrodynamic and water quality model using a three-layer nested structure grid for a heavy rainfall and flooding process in August 2022. The spatial and temporal response characteristics of the pollutant discharge process from the Tang River and the ecological environment of the estuary were examined.

2 Materials and methods

Delft3D is among the most advanced of the two-dimensional and three-dimensional hydrodynamics and water quality modeling systems available worldwide; it was developed by Delft Hydraulics (Deltares, formerly WL|Delft Hydraulics, Delft, the Netherlands). A three-scale nested grid was established, using Delft3D, to simulate the hydrodynamics (i.e., tidal current field, wave field), temperature–salinity field, and water quality in the Bohai Sea, Qinhuangdao coastal area, and the Tang Estuary. The results of the numerical model can

provide a basic background on the dynamic field and nutrient environment field for the study of biological growth and forecasting of ecological disasters in the Qinhuangdao coastal area.

2.1 Area and mesh

The finite volume method (FVM) and a structured grid were used to solve the two-dimensional shallow water equation, which mainly considered the tidal and wave action driven by the outer sea boundary and the wind field. For different water depth and sediment conditions, the bottom friction coefficient was introduced, and the dry and wet grid conditions were considered in the nearshore area. In order to describe the flow field and water level process, a triple-nested grid model was established, with the large regional scope of the Bohai Sea, medium regional scope of Qinhuangdao, and fine regional scope of the Tang Estuary (Figure 1). The number of nodes in each of the three scales of model was 249 × 315, 245 × 206, and 372 × 491, respectively. The corresponding grid resolutions were 1500 m, 350 m, and 15 m, respectively. The Dalian–Yantai line was treated as the outer boundary of the Bohai Sea, with water-level superimposition of the static pressure and the astronomical tide. The tide-level data were calculated *via* the tide wave model NAOTIDE, a data set of tide forecast, in the adjacent areas of Japan; the resulting data were verified by comparing them with tide-level data from the tide gauge station in the Bohai Sea. The tidal level and velocity process of the middle-level Qinhuangdao model was provided by the Bohai Sea model. The land boundary of the middle-level model was defined by 11 river estuaries, which were controlled by the measured monthly average runoff of these rivers. The tidal level and flow velocity of the Tang Estuary model were provided by the Qinhuangdao model. The land boundary of the fine-level model was defined by two river estuaries, the Tang River and its tributary Xiaotang River, which were controlled by measured flow velocity.

The model parameters comprised time step, Courant number [Courant–Friedrichs–Lewy (CFL) number], horizontal eddy viscosity coefficient, bed friction, and Coriolis force. The time steps of the triple-scale model were set at 30 s, 15 s, and 3.75–7.5 s. A CFL number below 0.8 was maintained by controlling the time step employed in different ranges, which can effectively solve the problem of model instability. The Manning number was 0.0163 $s/m^{1/3}$, in accordance with the bottom sediment particle size and water depth. The values of the horizontal eddy viscosity coefficient and the horizontal eddy diffusion coefficient were dependent on the grid size; these were set to 15 m^2/s and 100 m^2/s, respectively, in both the Bohai Sea model and the Qinhuangdao model, and to 1 m^2/s and 10 m^2/s, respectively, in the Tang Estuary model. The Coriolis force was determined by the latitude of the model region.

2.2 The hydrodynamic model

The governing equations are:

$$\frac{\partial h}{\partial t} + \frac{\partial hu}{\partial t} + \frac{\partial hv}{\partial y} = hS$$

$$\frac{\partial hu}{\partial t} + \frac{\partial hu^2}{\partial x} + \frac{\partial hvu}{\partial y} = fvh - gh\frac{\partial \eta}{\partial x} + \frac{\tau_{sx} - \tau_{bx}}{\rho} + \frac{\partial}{\partial x}(hT_{xx}) + \frac{\partial}{\partial y}(hT_{xy}) + hu_sS$$

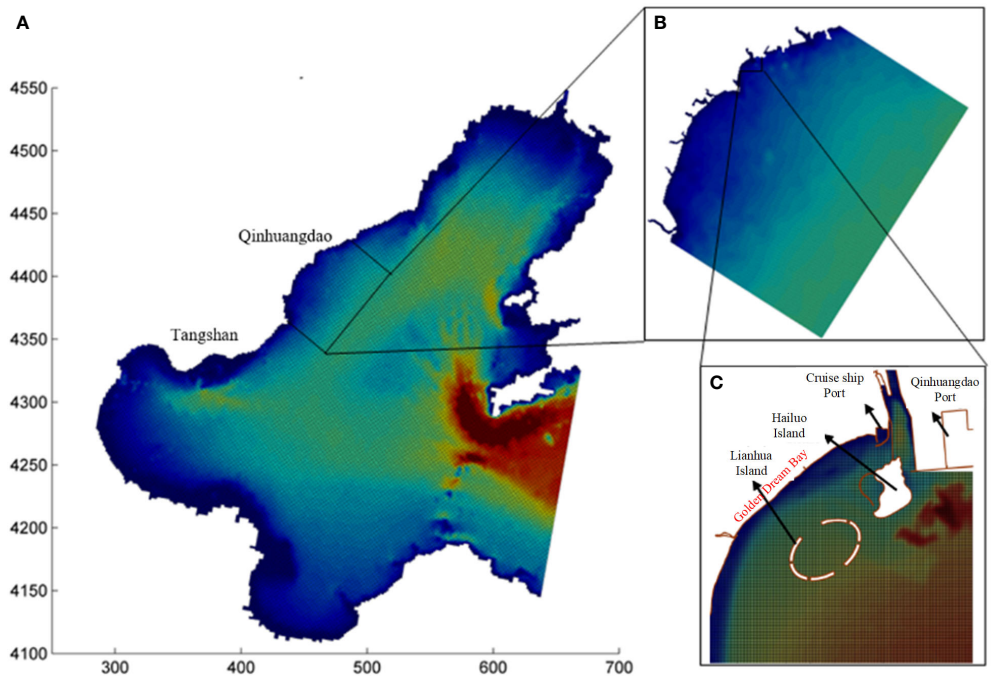

FIGURE 1
Area and mesh of the nested model: **(A)** the Bohai Sea, **(B)** the Qinhuangdao Coastal area, and **(C)** the Tang Estuary.

$$\frac{\partial hv}{\partial t} + \frac{\partial hv^2}{\partial y} + \frac{\partial hvu}{\partial x} = fuh - gh\frac{\partial \eta}{\partial y} + \frac{\tau_{sy} - \tau_{by}}{\rho} + \frac{\partial}{\partial x}(hT_{xy}) + \frac{\partial}{\partial y}(hT_{yy}) + hv_sS$$

where η is the water level, h is the total water depth, d is the static water depth, and $h = \eta + d$; t is time; u and v are the average velocity along water depth in the x and y directions, respectively; g is the acceleration of gravity; $f = 2\Omega sin\phi$ is the Coriolis force coefficient (Ω being the rotation rate of the Earth, and ϕ the geographic latitude); ρ is the density of the water; τ_{sx} and τ_{sy} represent wind stress in the x and y directions, respectively; τ_{Bx} and τ_{By} represent the bottom friction in the x and y directions, respectively; S is the source (sink) item; and u_s and v_s are the velocity components of the source (sink). The lateral stress term T_{ij} includes viscosity and turbulence.

2.3 The water quality model

The Delft3D water quality model can simulate sediment transport and water quality processes in large and medium-scale areas. The water quality model includes the convection–diffusion equation and a large standard equation library, corresponding to the selected material type, and the point source and area source of pollution diffusion processes. Coupled with the hydrodynamic results, the water quality model can calculate the dynamic distribution of concentrations of related materials and their derivatives in the water and sediment layers.

The two-dimensional transport equation is given in the form of convection diffusion, as follows:

$$\frac{\partial hT}{\partial t} + \frac{\partial huT}{\partial x} + \frac{\partial hvT}{\partial y} = hF_T + hH + hT_sS,$$

$$\frac{\partial hs}{\partial t} + \frac{\partial hus}{\partial x} + \frac{\partial hvs}{\partial y} = fF_s + hS_sS,$$

where T and s are the depth-averaged temperature and salinity, respectively; T_s and s_s are the horizontal diffusion terms for temperature and salinity, respectively; F_T and F_s are the source terms for temperature and salinity, respectively; and H indicates the source term for heat exchange between seawater and air.

The boundary conditions are important for the prediction of water quality during the period of heavy rain. Based on data from the online monitoring stations of the Tanghe River and Xiaotanghe River on terrestrial pollutants, the boundary conditions for the model concerning current speed and water quality were set as shown in Table 1.

2.4 Model verification

2.4.1 Verification of hydrodynamics

Verification of the tide and wave data were considered in the hydrodynamic model. Nine stations were designated for tide verification, including Yantai, Bayuquan, Jinzhou Port, Qinhuangdao, Jingtang Port, and Tanggu in the Bohai Sea (shown in Figure 2). Based on the time of occurrence of the extreme weather (heavy rainfall), the tide level data for 15 July to 15 August 2022 were collected from each of these gauge stations. The empirical data were harmonically analyzed as the measured value of the astronomical tide for comparison with the calculated values. Wave monitoring data for the period of 1 July to 1 September 2022 were also collected from each buoy in Qinhuangdao for validation of the model results. The error between the calculated value and the measured value was analyzed to evaluate the accuracy of the model and verify the reliability of the model for the coastal waters of Qinhuangdao.

TABLE 1 Boundary condition settings of the model.

Station	Time	Current (m/s)	NH_4-N (mg/L)	NO_3-N (mg/L)	PO_4-P (mg/L)
Tang River	18/8/2022 20:00:00	−0.01	0.10	2.39	0.02
	19/8/2022 00:00:00	−2.57	0.43	1.91	0.01
	19/8/2022 04:00:00	−4.29	0.33	1.80	0.03
	19/8/2022 08:00:00	−1.61	0.34	3.22	0.04
	19/8/2022 12:00:00	−0.78	0.30	3.93	0.03
	19/8/2022 16:00:00	−0.59	0.33	4.55	0.05
	19/8/2022 20:00:00	−0.36	0.25	5.03	0.04
Xiaotang River	18/8/2022 20:00:00	−0.23	0.69	5.49	0.08
	19/8/2022 00:00:00	−2.34	1.05	2.31	0.18
	19/8/2022 04:00:00	−1.94	0.59	1.81	0.16
	19/8/2022 08:00:00	−1.13	0.43	6.70	0.12
	19/8/2022 12:00:00	−0.68	0.45	5.87	0.13
	19/8/2022 16:00:00	−0.58	0.42	5.83	0.15
	19/8/2022 20:00:00	−0.42	0.43	6.72	0.13

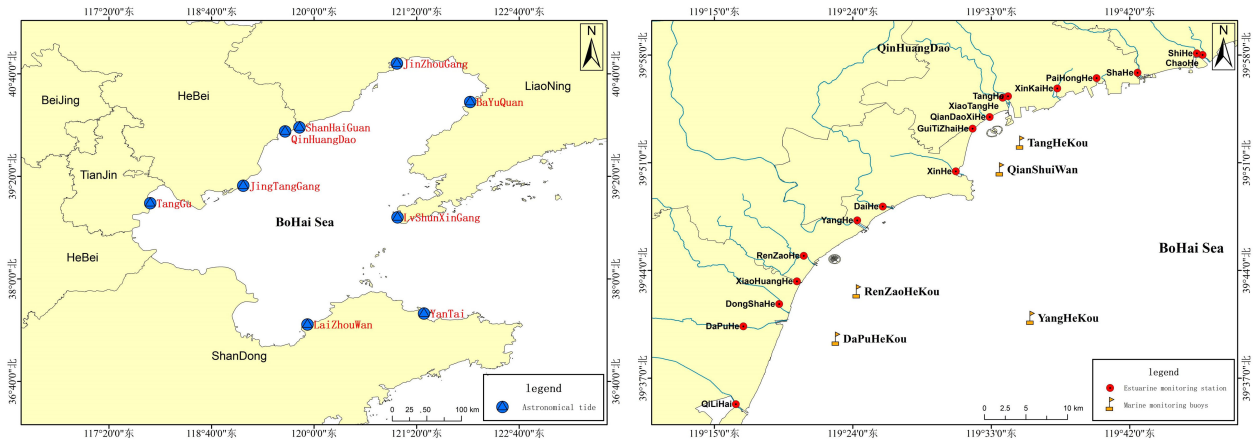

FIGURE 2
Gauge stations used for verification of the numerical model.

In order to obtain a better evaluation criterion than the common method, which uses the correlation coefficient and standard deviation, the Willmott statistical method was used to evaluate the simulation results of the model, as follows:

$$skill = 1 - \frac{\sum_{i=1}^{N}|M-D|^2}{\sum_{i=1}^{N}(|M-\bar{D}|+D-\bar{D}|)^2}$$

The Willmott statistical method takes into account the correlation between the deviation between the measured value D and the measured average value $\bar{D}$, and the deviation between the calculated value M and the measured average value $\bar{D}$. The resulting skill value ranges from 0 to 1. A value of 1 means that the result is completely consistent with the measured value; a value of 0.65–1 represents an excellent corroboration, 0.5–0.65 represents a very good corroboration, 0.2–0.5 represents a good corroboration, and 0–0.2 represents a poor corroboration.

As shown in Table 2, tide level verification indicated excellent model skill, with skill values of more than 0.86 at all the gauge stations; this proves that the model simulation values were in good agreement with the measured values. Verification of the tidal current and wave simulation values indicated that these were good, with skill values of more than 0.4 for selected ocean observation buoys.

As shown in Figure 3, the model can simulate the propagation of tidal waves in the Bohai Sea. Data plotted with dots represent the astronomical tides at typical tidal stations, whereas the black line represents the calculation results for tide amplitude and tide phase.

TABLE 2 Hydrodynamic model evaluation.

Variable	Time	Station	Skill	Performance
Tidal level	15 July–15 August 2011	Yantai	0.95	Excellent
		Lvshunxingang	0.98	Excellent
		Bayuquan	0.99	Excellent
		Jinzhougang	0.99	Excellent
		Shanhaiguan	0.94	Excellent
		Qinhuangdao	0.92	Excellent
		Jingtanggang	0.97	Excellent
		Tanggu	0.98	Excellent
Speed	29 July–1 August 2022 and 12 August–15 August 2022	Yanghekou	0.54	very good
Direction	18 July–23 July 2022	Yanghekou	0.48	good
Effective wave height	1 July–24 August 2022	Tanghekou	0.56	very good
		Yanghekou	0.45	good
		Renzaohekou	0.45	good
		Dapuhekou	0.48	good

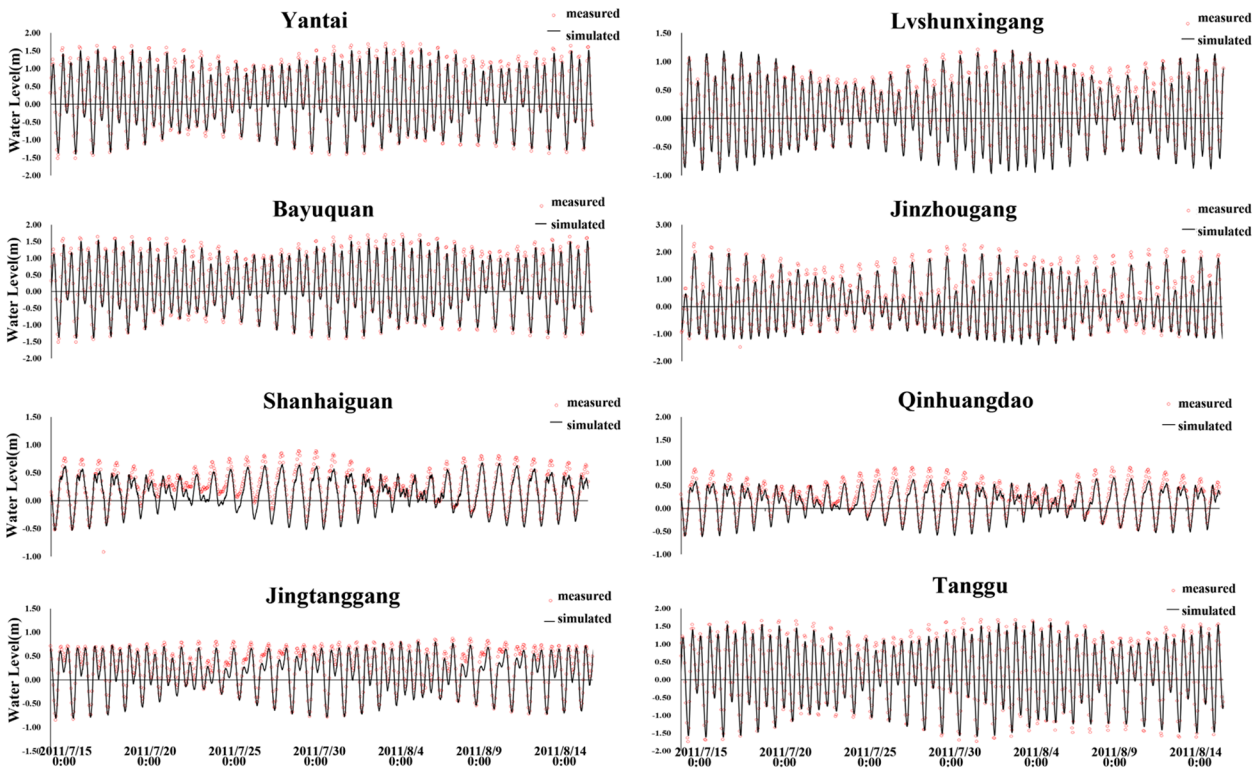

FIGURE 3
Verification of tidal level.

The calculated values are in good agreement with the predicted values for amplitude and phase. Figures 4, 5 show that the simulation results for velocity and wave height were also acceptable.

2.4.2 Water quality verification

Three concentration parameters were used to evaluate the water quality: nitrate-nitrogen, ammonium-nitrogen, and ortho-phosphate (NO_3-N, NH_4-N, and PO_4-P, respectively). These parameters have a significant impact on the growth of algae, and their verification is shown in Figure 6. The data were obtained during the period 15–31 August 2022 at the water quality and nutrient observation buoy in Qinhuangdao coastal waters (shown in Figure 2).

As illustrated, the simulated results fit well with the measured ones, with skill values for NO_3^-, NH_4^+, and PO_4^{-3} of 0.96, 0.93, and 0.93, respectively. The simulated values were very close to the measured values, and can be used to provide the basic background in terms of

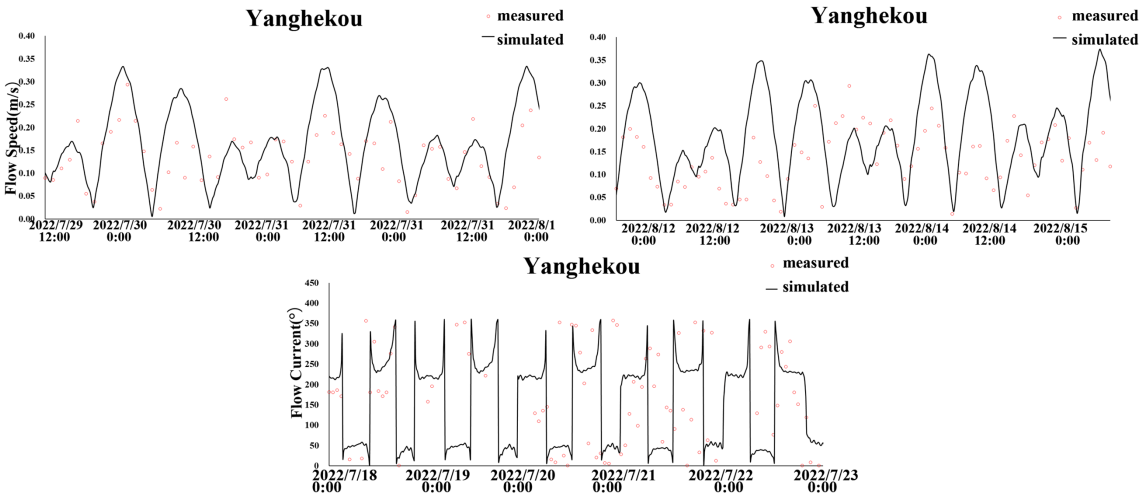

FIGURE 4
Verification of flow velocity.

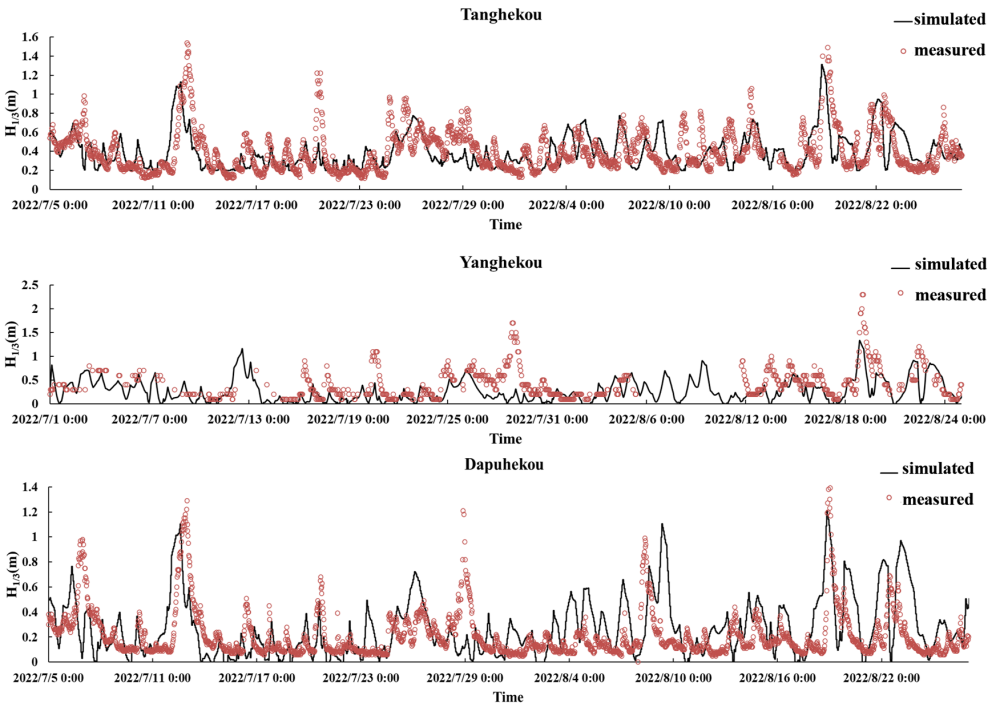

FIGURE 5
Verification of wave height.

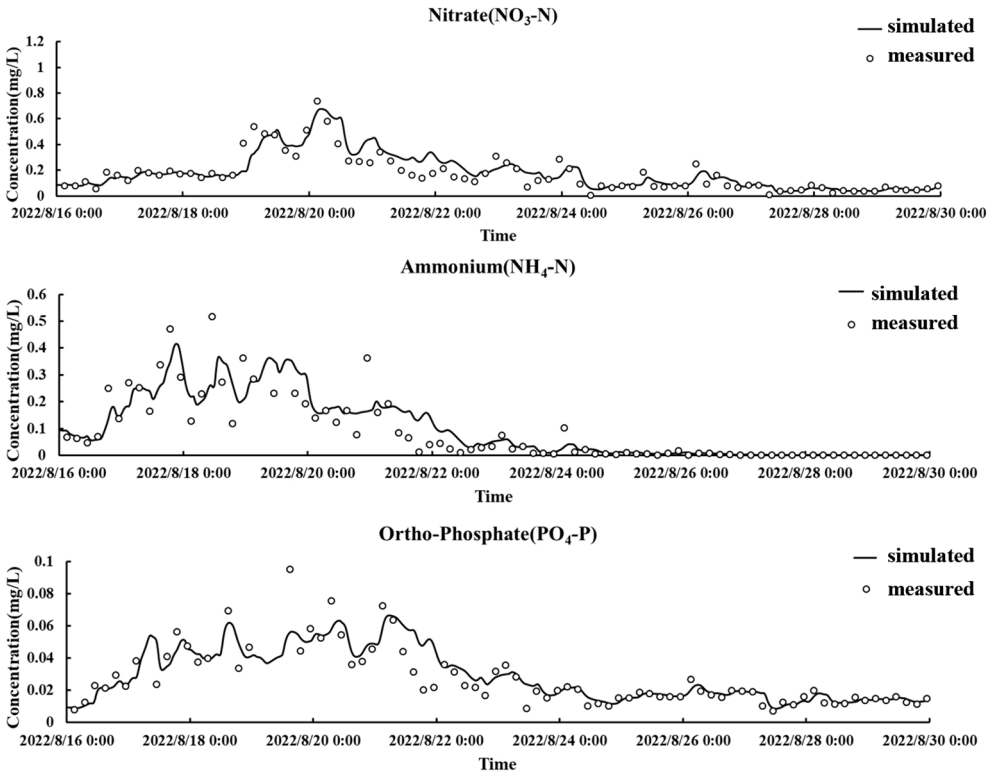

FIGURE 6
Water quality verification.

the dynamic field and environmental field for the study of the warning signs and forecasting of ecological disasters in Qinhuangdao coastal waters.

3 Results

3.1 Discharge of riverine pollutants into the sea as a result of heavy rainfall

In this study, data on the water quality and riverine discharge of the Tang River were collected from the online marine ecological monitoring station at intervals of 4 h. Figure 7 shows the changes in concentration of pollutants during the flood discharge of the Tang River. On the night of 18 August 2022, the riverine discharge of the Tang River into the sea increased rapidly owing to heavy rainfall. At 04:00 on 19 August, the discharge reached its maximum level of 295.4 m^3/s. The discharge then decreased rapidly to 48.6 m^3/s by 12:00,, until 08:00 on 20 August, when the discharge returned to the same magnitude as before the rainfall. At this time, the concentrations of pollutants, as indexed by measures such as chemical oxygen demand (COD), dissolved inorganic nitrogen (DIN), and dissolved total nitrogen (DTN), fell to pre-rainfall levels, and the flooding process ended. As can be seen in Figure 7, the water quality of the Tang River changed as a corroboration of the period of rainfall. The overall pollutant concentrations were all higher than before the rainfall. Different pollutants exhibited different responses; among these, COD and NH_4-N rose and fell consistently with the flow discharge. The concentration of COD reached a maximum value of 37.293 mg/L at 04:00 on 19 August and then decreased rapidly, while NH_4-N reached a maximum concentration of 0.427 mg/L at 0:00 on 19 August and then slowly fluctuated downward. The concentrations of DIN, DTN, and NO_3-N decreased slightly at first, then increased gradually, and gradually stabilized. The concentration of DTP gradually increased during the flooding process and then stabilized at approximately 0.11 mg/L. Finally, the concentrations of PO_4-P and

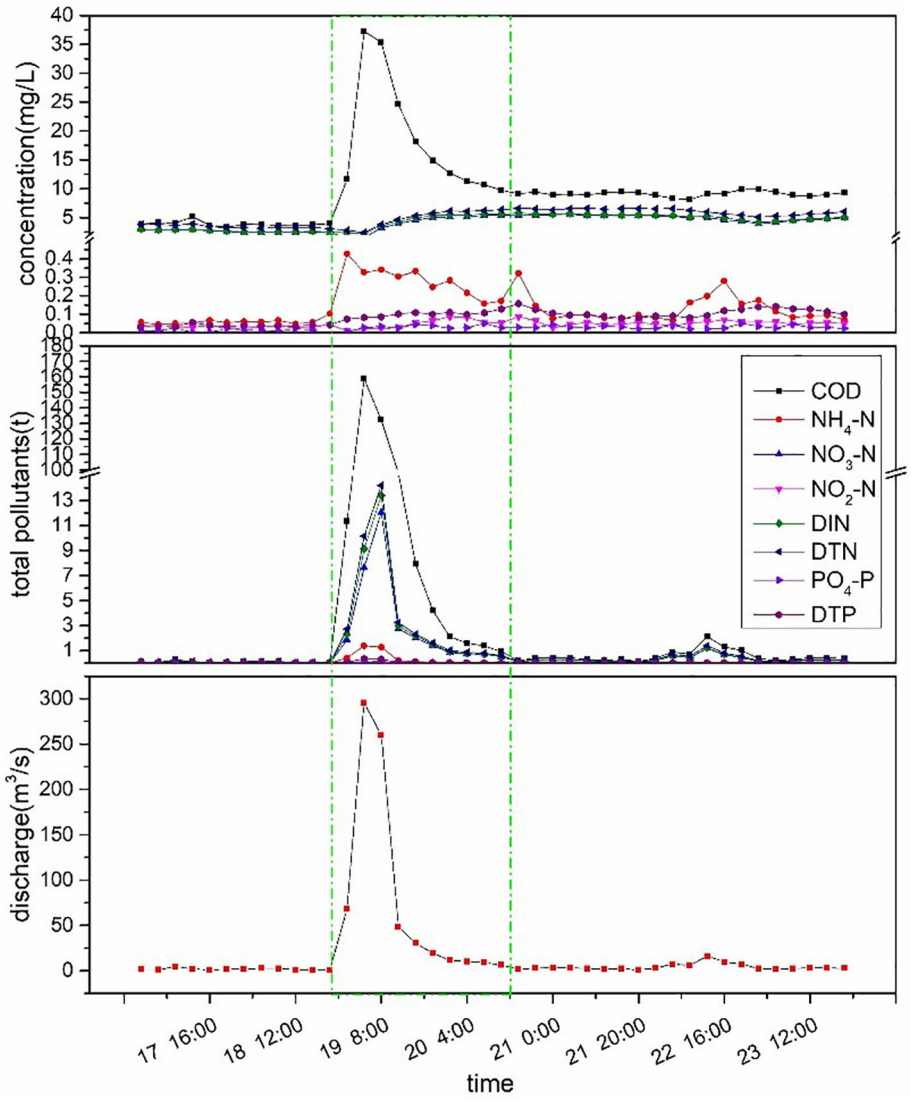

FIGURE 7
Flooding process of the Tang River caused by heavy rainfall in August 2022. DIN: dissolved inorganic nitrogen.

NO_2-N exhibited a fluctuating tendency to increase. The monitoring data indicated that during the flooding process, the changes in the total amount of each pollutant were mainly determined by the flow discharged, given these consistent trends. The total flux of flood water was 1098.86×10^5 m^3; the total amount of DIN discharged into the sea was 37.97 t, mainly consisting of 30.84 t of NO_3-N and 3.21 t of DON. The total amount of DTP discharged into the sea was 0.96 t, consisting of 0.64 t of DOP and 0.32 t of PO_4-P. Finally, the overall ratio of nitrogen to phosphorus in the discharged flood water was approximately 48:1.

3.2 Hydrodynamic responses

As a result of the flood water flow induced by the period of heavy rainfall, the coastal hydrodynamics in the Tang Estuary were significantly changed (shown in Figure 8). The flow velocity in the west coastal area of the Tang River channel was relatively higher. In the east coastal area, vortexes of varying sizes were formed by the blocking of the discharging flow by Hailuo Island, the port breakwater, and the Tongdao Bridge. The discharging flow was divided into two component currents by Hailuo Island. Current A moved southwest along the shore under the Tongdao Bridge to reach the Golden Dream Bay, causing a 180° transition of the tidal flow on the landward side of Lianhua Island. Current B moved offshore along the channel between Hailuo Island and the port breakwater, where the hydrodynamics on the seaward side of the island underwent no significant changes. With the increasing discharge from the Tang River into the sea, the vortexes on the east coast became larger with decreased number. Meanwhile, the current flow velocity on both sides of Hailuo Island increased significantly, with a larger influencing range. Current A, constrained by the tourist port breakwater and Hailuo Island, formed a clockwise vortex in the Golden Dream Bay, and current B began to affect the external area on the southeast side of Hailuo Island. At 03:00 on August 19, the flood water reached the maximum range of the hydrodynamic environment. The two vortexes on the east side of the Tang River channel and the west side of the port breakwater became much larger. The impact of current A significantly exceeded the landward shelter area of the two islands, where the flow velocity near the islands was higher and gradually decreased landwards. The hydrodynamics on the seaward side of the two islands were mainly influenced by current B, which changed its direction in the area southeast of Hailuo Island and flowed southwest along the seaward side of the two islands. The velocity gradually decreased, and the current was deflected at the southwest end of

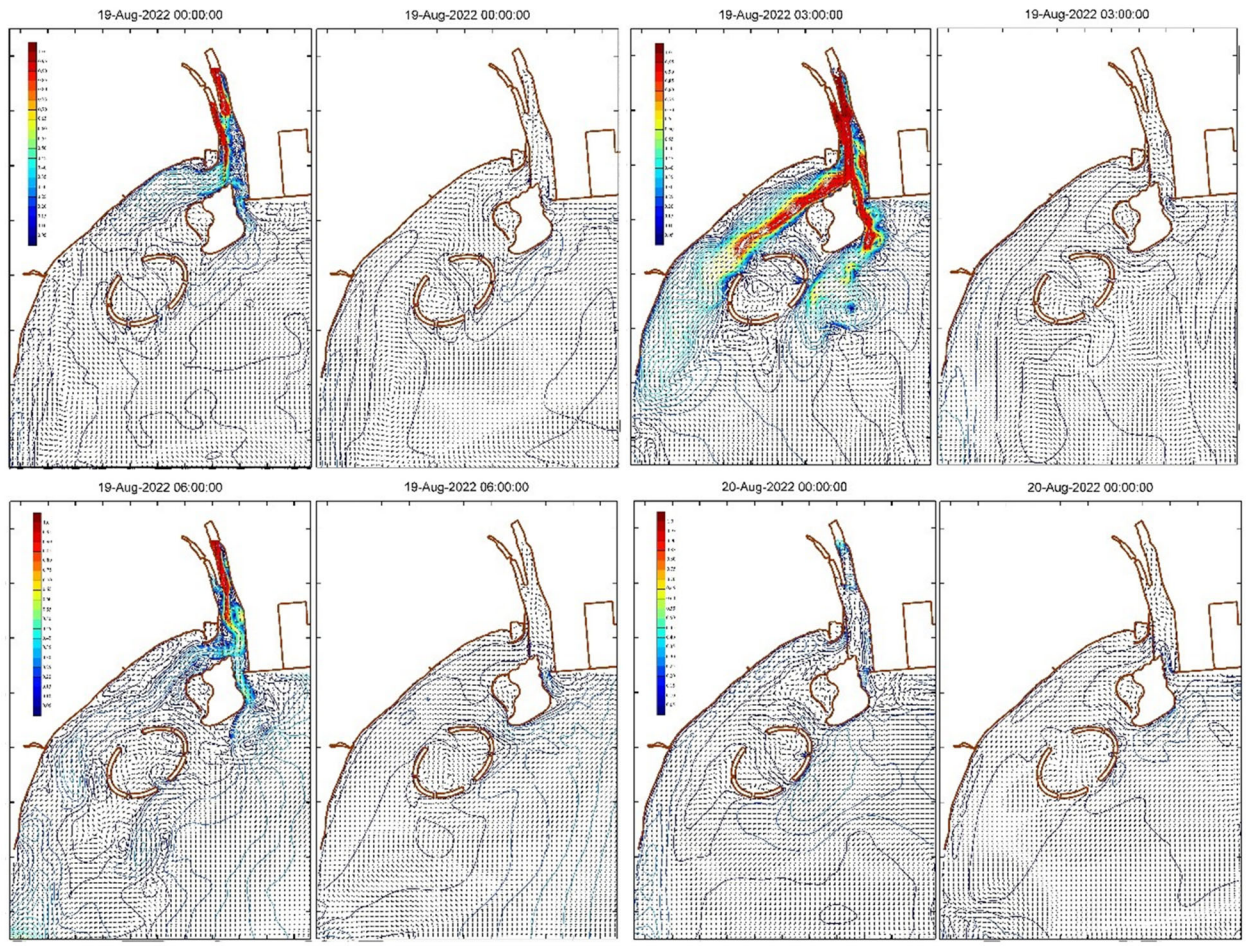

FIGURE 8
Hydrodynamic responses caused by heavy rainfall in August 2022.

Lianhua Island under the influence of open sea dynamics. With the gradual reduction of the flow discharge, the effects on the hydrodynamics in the Tang Estuary were also gradually weakened. At 06:00 on 19 August, because of the significantly weakened state of current A on the land side of the islands, a larger vortex formed under interaction with the falling tide. With the continuous reduction of the discharging flow of the Tang River, the hydrodynamics became more complex owing to the joint action of the runoff flow and the tide in the Tang Estuary. After 11:00 on 19 August, the hydrodynamics in the Tang Estuary were mainly determined by the rising or falling tide. At 18:00 on 19 August, the hydrodynamics on the sea side of the islands were in complete accordance with the rising and falling tide, while the runoff flow was only visible from the land side of the islands and was mainly limited to the river channel.

3.3 Pollutant migration and dispersion during flood discharge

The flooding of the Tang River drained a large quantity of pollutants into the sea and ocean. This paper presents a simulation of the migration and dispersion processes of the major inorganic nutrients (DIN, NO_3-N, NH_4-N, and PO_4-P) that damage the marine ecological environment. Following this simulation, the responses of the water environment to the pollutants draining out were then investigated.

The overall changes of the concentrations of DIN and NO_3-N were found to have broadly the same distribution, as shown in Figures 9, 10. At 00:00 on 19 August, the water from the upstream river rapidly entered the estuary channel, at which time the concentrations of DIN and NO_3-N also increased rapidly. The concentrations of DIN and NO_3-N at the river mouth were greater than 3 mg/L and 2 mg/L, respectively. The concentrations on the landward side of Hailuo Island and in the sea area on the side of the port breakwater decreased gradually from the Tang Estuary to the outer sea. Owing to the dramatic increase in flood water flow into the sea, the scope of influence of DIN and NO_3-N was enhanced. At 01:00 on 19 August, the concentrations of DIN and NO_3-N on the landward side of Hailuo Island and Lianhua Island were greater than 2 mg/L and 1.5 mg/L, respectively, while the concentrations on the seaward side began to increase. At 03:00, the concentrations of DIN and NO_3-N were greater on the landward side of the islands than on the seaward side; there was a gradual decrease in concentration from the shore to the sea. The concentrations showed a trend of decreasing from the Tang Estuary along both sides of the coast. The areas of maximum concentration of DIN and NO_3-N in the Golden Dream Bay coincided with the vortex area formed by the hydrodynamics at this time. At 06:00 on 19 August, the concentrations of DIN and NO_3-N began to gradually increase again. Influenced by the flood water flow and tidal power, the dispersion of DIN and NO_3-N migration increased on the landward side of the islands, while decreasing on the

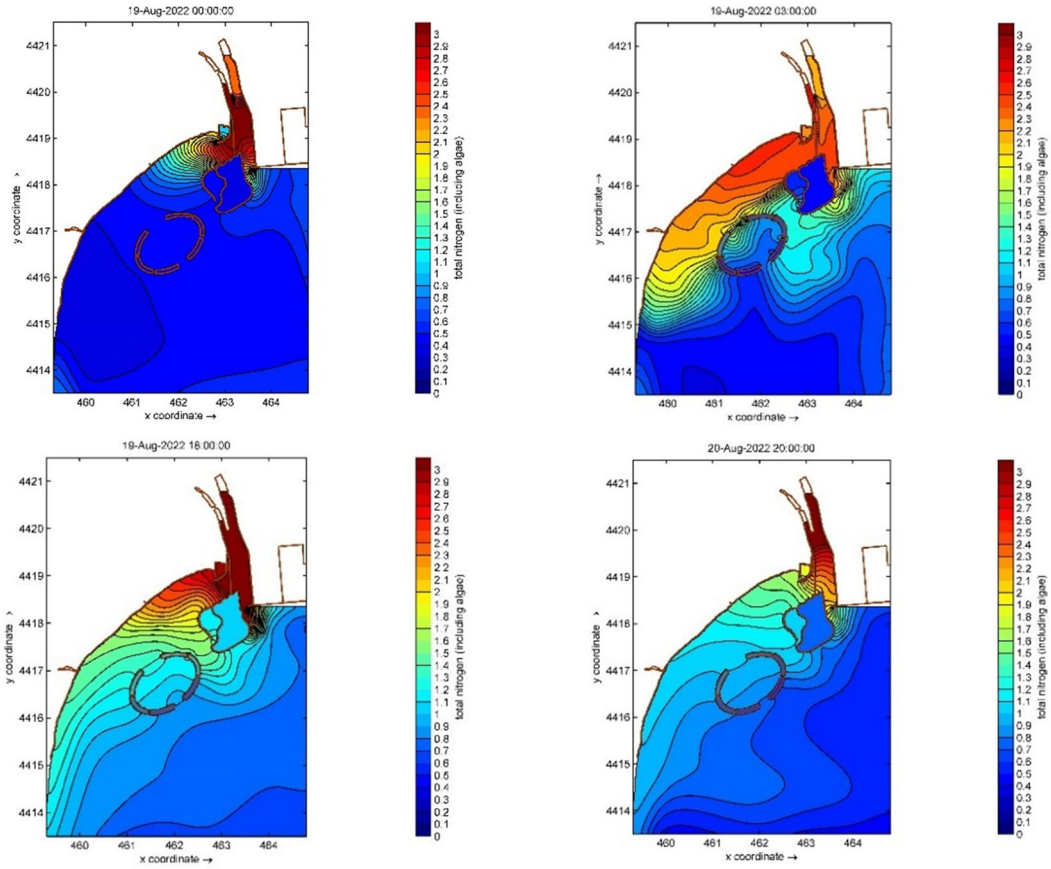

FIGURE 9
The process of diffusion of dissolved inorganic nitrogen (DIN) in the Tang Estuary caused by heavy rainfall in August 2022.

seaward side. The range of high DIN and NO_3-N concentration was affected by the reduction in the flood water flow, with a gradual decrease in their distribution. By 18:00 on 19 August, the concentrations of DIN and NO_3-N on the landward side of the islands and in the area between the two islands were greater than 1 mg/L and 0.8 mg/L, respectively. The high concentrations of DIN and NO_3-N were mainly concentrated in the river channel at the estuary. After this point, the concentrations around the islands began to gradually decrease. At 00:00 on August 20, the concentrations outside the islands had essentially dropped to their pre-flooding levels. With the further reduction of the runoff flow, the influence of tides increased to form a high concentration in source area of DIN and NO_3-N at the river mouth. At this point, the dynamics of migration were dominated by the tidal power rather than the flood water flow. By 16:00 on 20 August, the effects of the Tang River flooding had almost entirely disappeared. At 10:00 on 25 August, the high concentrations of DIN and NO_3-N in the source area had returned to pre-flood levels under the influence of tidal currents. Following this flooding process, the impact of DIN and NO_3-N discharging into the sea lasted for approximately 6.5 days.

The pollutants NH_4-N and PO_4-P were mainly discharged from the Xiaotang River, a tributary of the Tang River. The overall characteristics of the discharge of these pollutants differed from those of the discharge of DIN and NO_3-N (shown in Figures 11 and 12). During the initial stage of flooding, the concentrations of these pollutants in the main channel of the upper Tang River were low. In contrast, concentrations in the Xiaotang River were very high, causing a rapid increase in the estuary, with concentrations of NH4-N and PO4-P greater than 0.4 mg/L, and 0.06 mg/L,respectively. At 01:00 on 19 August, the flood water flow in the main channel increased rapidly, and the concentrations of NH_4-N and PO_4-P in the estuary decreased. The concentrations on the landward side of the two islands and the seaward side of Hailuo Island increased rapidly. At 03:00 on 19 August, the pollutants on the landward side of the two islands migrated continuously in a southwesterly direction, with concentrations on the landward side significantly greater than those on the seaward side. Subsequently, the concentrations of the pollutants decreased continuously. At 06:00 on 19 August, the concentrations of NH_4-N and PO_4-P in the river channel decreased rapidly to 0.035 mg/L, and 0.035 mg/L, respectively. The contours of these concentrations were broadly the same as the coastal direction. In the direction normal to the shoreline, the concentrations showed a trend of gradually decreasing, and migrated and spread out to the sea under the influence of the tidal power. By 00:00 on 20 August, the concentrations were broadly the same as the baseline ocean values. The total duration of the diffusion process was approximately 1 day.

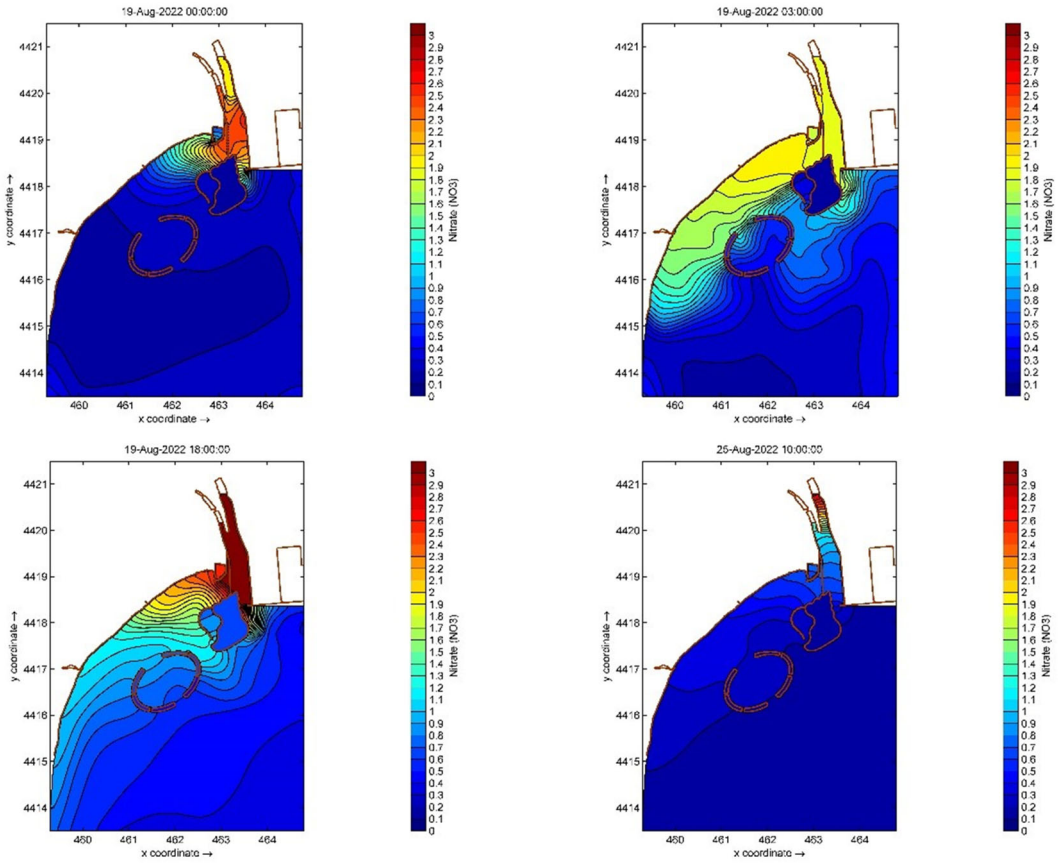

FIGURE 10
Nitrate-nitrogen (NO_3-N) diffusion process in the Tang Estuary caused by heavy rainfall in August 2022.

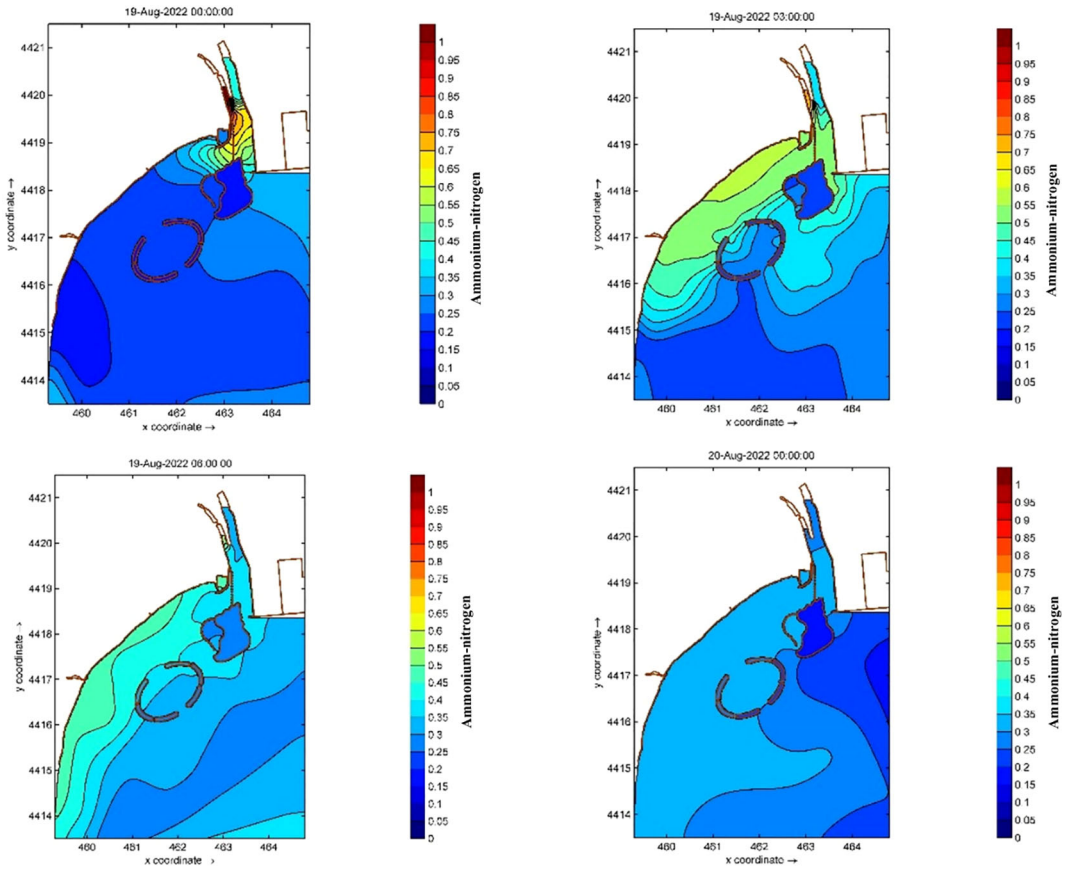

FIGURE 11
The process of diffusion of NH_4-N in the Tang Estuary caused by heavy rainfall in August 2022.

4 Discussion

4.1 Response modes for pollutant discharge into the sea

Under weak tidal dynamics, the short-term responses of pollution discharge into the sea can be roughly divided into two modes according to the formation of high concentrations in the source area, namely "rapid migration by the flood water flow + diffusion of a high concentration in the source area" and "rapid migration by the flood water flow + diffusion by the tide".

In this study, the diffusion patterns of DIN and NO_3-N were found to follow the first mode. During the stage of rapid migration by the flood water flow, the coastal area is mainly influenced by the flood flow of the river (Gu et al., 2017). Pollutants migrate rapidly with the flood water flow, and the concentration shows a trend of an initial high level, followed by a decrease, and then an increase again. This trend is related to the heavy rainfall and upstream pollutant release process (Kuang et al., 2015). During the stage in which the flood waters fall, pollutant diffusion enters the second stage, characterized by diffusion of the high concentration in the source area by tidal power. In this case, owing to the presence of complex artificial constructions, the estuary forms a relatively closed area meaning that the pollutant concentration in the area is high (Makabe et al., 2014; Kuang et al., 2019), forming a pollutant source area. This pollutant source area becomes another fixed pollutant source, slowly diffused under tidal power. The diffusion time of this pollutant source is much longer than the rapid migration occurring in the case of the flooding current, with the ratio of the durations of the two stages being approximately 1:5.5.

In contrast, the diffusion patterns of NH_4-N and PO_4-P were found to follow the second stage. At the early stage of flooding, high concentrations can be found in the flooding water. Under the action of the flood water flow, the pollution rapidly migrates and disperses in the coastal area, with the concentrations gradually decreasing or fluctuating slightly (Cao et al., 2017). With the decreasing flood flow, the pollutant dispersion process shifts to become dominated by tidal power, at which point the concentrations are essentially returning to pre-flooding levels, without forming an obvious "high concentration in the source area". With the further reduction of the flood water flow, the impact on these pollutants gradually ceases entirely.

As shown in Table 1, according to the field observations, NH_4-N and PO_4-P mainly come from the Xiaotang River, a tributary of the Tang River. When the small runoff from the Xiaotang River carries these pollutants into the Tang River, the large flow of the main stem disperses the concentration of these pollutants. With the concentration diluted, the pollutants are more easily carried away by the main stem to discharge into the sea. Therefore, a high concentration cannot form in the source area. In contrast, NO_3-N

comes from both the main stem of the Tang River and the Xiaotang River. The inflow of the Xiaotang River leads to a further increase in NO_3-N concentration in the estuary. Moreover, with the continuous water supply, the concentration of the pollutant in the estuary cannot easily be dissipated. Thus, a high concentration can form in the source area.

4.2 Responses in the form of eco-toxicogenic algal disaster

Studies have shown that most harmful algal blooms in coastal waters around the world are related to eutrophication (Fletcher, 1996; Valiela et al., 1997; Anderson et al., 2002; Heisler et al., 2008). Ecological disasters such as red and green tides occur frequently on the coast of Qinhuangdao. The growth of the causative algae is closely related to the pollutant diffusion, hydrodynamics, and meteorology of the Tang River (Cao et al., 2017; Han et al., 2019; Song et al., 2019; Zhang WL. et al., 2020; Han et al., 2022; He et al., 2022).

The Golden Dream Bay is the main area of Qinhuangdao where ecological disasters such as red and green tides occur (Kuang et al., 2021; Han et al., 2022). Figure 13 shows the changes in biomass of red tide and green tide algae species before and after the period of heavy rainfall examined here. The biomass of these species in the Golden Dream Bay decreased sharply during the rapid migration stage of the flooding current, although the concentration of nutrients (i.e., N and P) increased rapidly. This was caused by the high velocity of the flood water flow, which destroyed the habitat of the algal species that produce red and green tides (Han et al., 2019). With the gradual weakening of the flood water flow, the biomass of algae increased dramatically under the suitable environmental conditions of tidal power and high concentrations of nutrients (Pedersen and Borum, 2010). The high-concentration source area serves as an additional source of nutrient salts and prolongs the time span of the local eutrophication. These high-concentration nutrient salts also provide a continuous source of growth and reproduction of biomass for red tide and green tides. It can be concluded that this is one of the main reasons why ecological disasters such as red and green tides often occur 1–5 days after heavy rainfall.

4.3 The influence of the Tongdao Bridge on coastal water quality

The ecological environment of the bay area near the estuary is very vulnerable to flooding of the river. During the flooding caused by heavy rainfall, the river not only brings a large amount of pollutants into the sea, but also carries a large amount of land-based waste material, which accumulates on the bay beach and damages the beach's usability for bathing.

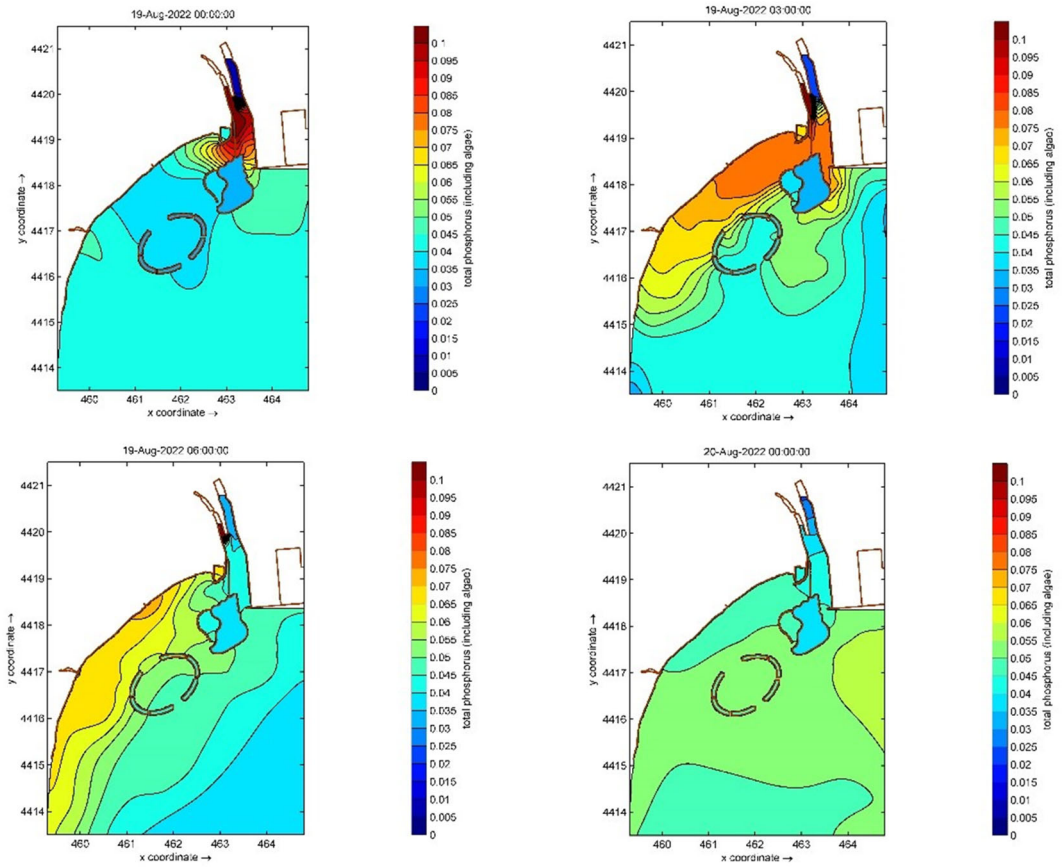

FIGURE 12
The process of diffusion of PO_4-P in the Tang Estuary caused by heavy rainfall in August 2022.

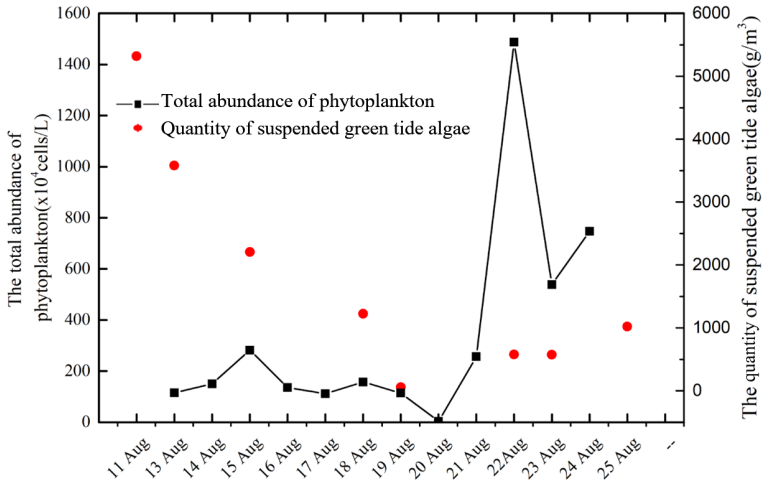

FIGURE 13
Changes in red tide and green tide biomass in August 2022.

From the hydrodynamic simulation, it can be seen that, in the Tang Estuary, the overall hydrodynamic conditions are weakened by the fact that the Tongdao Bridge reduces the cross-section area between Hailuo Island and the mainland. This reduces the diffusion rate of pollutants from the river (Kuang et al., 2019). The bridge may negatively affect the water quality of the Golden Dream Bay bathing beach under conventional ocean dynamics (Sheng et al., 2016). During short-term flooding of the Tang River, a large amount of land-based waste material may be deposited on the bathing beach adjacent to the path of the flood water under the bridge. The presence of the bridge leads to the accumulation of a large amount of land-based waste material, such as plant stalks, dead grass, domestic waste, and farming nets, on the Golden Dream Bay beach. The reduction in the water-crossing area by the bridge may play a certain beneficial role in maintenance of the water quality and in interdiction of the accumulation land-based waste material on the Golden Dream Bay bathing beach. At the same time, the bridge exerts a certain flow-guiding effect, so that some of the land-based pollutants and garbage drain into the sea through the channel between the Hailuo Island and Qinhuangdao Port breakwaters. On the basis of future hydrodynamics calculations, the construction of movable sluice gates under the bridge could be considered. The sluice gates could provide scientifically calculated and reasoned control over the water-crossing section of the bridge during the early rapid migration stage of the influx of flood water, so that the flood water could be directed into the channel between Hailuo Island and Qinhuangdao Port. This measure could reduce the pressures on the ecological environment, such as poor water quality and the presence of land-based waste material in the Golden Dream Bay.

5 Conclusions

The main objective of this study was to investigate the hydro-environmental responses of a weak tidal estuary to heavy rainfall, based on the analysis of field observation data and a numerical simulation. The modes of response to pollutant discharge, eco-toxicogenic algal disasters, and effects of permeable buildings on pollutant dispersion have been discussed. The main conclusions can be summarized as follows:

1. The quality of the discharging water was altered by the heavy rainfall. Overall pollutant concentrations were all higher than those occurring before the rainfall, but each pollutant responded with different changes. The trends in COD and NH_4-N concentrations were broadly the same as those in the flood water flow. The concentrations of DIN, DTN, and NO_3-N all decreased slightly, then gradually increased, and finally stabilized. The concentrations of PO_4-P and NO_2-N showed a lightly fluctuating trend toward increasing.

2. The hydrodynamic simulations showed that the flood water flow induced by heavy rainfall caused significant changes in the hydro-environment in the Tang Estuary. The coastal flow velocity increased on the west side of the river channel. Multi-scale vortexes were formed on the east side. As the flooding flow increased, the nearshore flow velocity further increased, and the vortexes became larger with decreased number.

3. The concentrations of typical pollutants in the estuary were closely related to the river flooding process. The concentrations of DIN and NO_3-N increased rapidly with the flooding. The diffusion of these two pollutants was very limited because of their high concentration in the source area. Normalization of these concentrations lagged behind the flooding process by approximately 5.5 days. In contrast, the diffusion of NH_4-N and PO_4-P occurred significantly more quickly because of the origination of these pollutants from the tributary and the fact that a high concentration did not accumulate in the source area.

4. Two short-term response modes for pollutant diffusion have been proposed. The two modes provide a viewpoint for exploration the role of changes in the hydro-environment in terms of offshore algal hazards and the effects of permanent structures on pollutant dispersion.

Data availability statement

The original contributions presented in the study are included in the article/supplementary material. Further inquiries can be directed to the corresponding authors.

Author contributions

GW: investigation, methodology, and writing of the original draft. XF: investigation, methodology, and validation. JZ: funding acquisition, resources, and supervision. ZH: funding acquisition, supervision, visualization, and writing of the original draft. YB: conceptualization and supervision. WS: resources. HX: writing of the original draft. All authors contributed to the article and approved the submitted version.

Funding

This work is supported by the National Key R&D Program of China (2019YFC1407905), the Key R&D Program of Hebei Province (21373302D), the National Natural Science Foundation of China (No. 52109097), and the Opening Fund of State Key Laboratory of Hydraulic Engineering Simulation and Safety (HESS-2226).

Acknowledgments

The author would like to thank Hebei Marine Environment Laboratory for the observed data for verification.

Conflict of interest

The authors declare that the research was conducted in the absence of any commercial or financial relationships that could be construed as a potential conflict of interest.

Publisher's note

References

Anderson, D. M., Glibert, P. M., and Burkholder, J. M. (2002). Harmful algal blooms and eutrophication: Nutrient sources, composition, and consequences. *Estuaries* 25, 704–726. doi: 10.1007/BF02804901

Cao, X. H., Yu, Z. M., Song, X. X., Yuan, Y. Q., Wu, Z. X., and He, L. Y. (2017). Pollution and discharge from tributaries to the Sea along qinhuangdao Coast:Impact on the bioactive elements related to brown tide outbreak. *Oceanol Et Limnol Sin.* 48 (5), 970–981. doi: 10.11693/hyhz20170300077

Conley, D. J. (2000). Biogeochemical nutrient cycles and nutrient management strategies. *Hydrobiologia* 410, 87–96. doi: 10.1023/A:1003784504005

Fletcher, R. L. (1996). "The occurrence of "green tides", a review," in *Marine benthic vegetation: recent changes and the effects of eutrophication*. Eds. W. Schramm and P. H. Nienhuis (Berlin: Springer-Verlag), 7–43.

Gu, J., Hu, C. F., Li, Z. Y., Kuang, C. P., Zhang, Y. F., et al. (2017). Coupling simulation and analysis of hydrodynamics and water quality in qinhuangdao rivers and coastal waters. *Mar. Sci.* 41 (2), 1–11. doi: 10.11759/hykx20160815001

Han, H. B., Li, Y., Ma, X. J., Song, W., Wang, Z. L., and Zhang, X. L.. (2022). Factors influencing the spatial and temporal distributions of green algaemicro-propagules in the coastal waters of jinmenghaiwan, qinhuangdao, China. *Mar. pollut. Bull* 175, 113328. doi: 10.1016/j.marpolbul.2022.113328

Han, H. B., Song, W., Wang, Z. L., Ding, D. W., Yuan, C., Zhang, X. L., et al. (2019). Distribution of green algae micropropagules and their function in the formation of the green tides in the coast of qinhuangdao, the bohai Sea, China. *Acta Oceanol Sin.* 38 (8), 72–77. doi: 10.1007/s13131-018-1278-1

Han, X. R., Wang, X. L., Sun, X., Shi, X., , Y., Zhu, C. J., Zhang, C. S., et al. (2003). Nutrient distribution and its relationship with occurrence of red tide in coastal area of East China Sea. *Chin. J. Appl. Ecol.* 14 (7), 1097–1101. doi: 10.13287/j.1001-9332.2003.0245

He, Y. K., Chen, Z. Y., Feng, X., Wang, G. Y., Wang, G., and Zhang, J. B. (2022). Daily samples revealing shift in phytoplankton community and its environmental drivers during summer in qinhuangdao coastal area, China. *Water* 14, 1625. doi: 10.3390/w14101625

Heisler, J., Glibertm, P. M., Burkholder, J. M., Anderson, D., Cochlan, W., Dennison, W., et al. (2008). Eutrophication and harmful algal blooms: A scientific consensus. *Harmful Algae* 8, 3–13. doi: 10.1016/j.hal.2008.08.006

Kuang, C. P., Hu, C. F., Mao, X. D., and Gu, J.. (2015). Numerical simulation of hydrodynamics and pollutant transport in qinhuangdao coastal water in the flood season. *J. Tongji Univ. (Natural Science)* 43 (9), 1355–1366.

Kuang, C. P., Wang, D., Zhao, F., Liu, H. X., and Zhu, L. (2021). Temporal and spatial distribution characteristics of water environmental factors in jinmeng bay and its adjacent waters. *J. Tongji Univ. (Natural Science)* 49 (6), 880–890. doi: 10.11908/j.issn.0253-374x.21008

Kuang, C. P., Yu, L. L., Gu, J., Dong, Z. C., Song, H. L., Zhu, L., et al. (2019). Influences of artificial island on water exchange of jinmeng bay. *China Environ. Sci* 39 (2), 757–767. doi: 10.19674/j.cnki.issn1000-6923.2019.0093

Lappalainen, A., and Ponni, J. (2000). Eutrophication and recreational fishing on the Finnish coast of the gulf of Finland, a mail survey. *Fish Manag Ecol.* 7, 323–335. doi: 10.1046/j.1365-2400.2000.007004323.x

Liu, X. H. (2010). Analysis on environment situation of coastal areas of bohai Sea. *Environ. Prot. Sci.* 36 (1), 14–18. doi: 10.16803/j.cnki.issn.1004-6216.2010.01.005

Liu, J., Liu, L. S., and Zheng, B. H. (2017). Problems and countermeasures of water environmental management in estuaries. *Res. Environ. Sci.* 30 (5), 645–653. doi: 10.13198/j.issn.1001-6929.2017.02.28

Luan, W. X., Wang, H., and Kang, M. J. (2016). *Study on the integrated zoning and control of pollution pressure in bohai rim region* (Beijing: Ocean Press).

Lucas, C. H., Graham, W. M., and Widmer, C. (2012). Jellyfish life histories: Role of polyps in forming and maintaining scyphomedusa populations. *Adv. Mar. Biol.* 63, 133–96. doi: 10.1016/B978-0-12-394282-1.00003-X

Makabe, R., Furukawa, R., Takao, M., and Uye, S.. (2014). Marine artificial structures as amplifiers of aurelia aurita s.l. blooms: a case study of a newly installed floating pier. *J. Oceanogr* 70, 447–455. doi: 10.1007/s10872-014-0249-1

Meybeck, M. (1982). Carbon, nitrogen, and phosphorus transport by world rivers. *Am. J. Sci.* 282, 401–450. doi: 10.2475/ajs.282.4.401

Pan, Y., Kuang, C. P., Chen, Y. P., Yin, S., Yang, Y. B., and Yang, Y. X.. (2018). A comparison of the performance of submerged and detached artificial headlands in a beach nourishment project. *Ocean Eng* 159, 295–304. doi: 10.1016/j.oceaneng.2018.04.038

Pan, Y., Yin, S., Chen, Y. P., Yang, Y. B., Xu, C.Y., and Xu, Z. S. (2022). An experimental study on the evolution of a submerged berm under the effects of regular waves in low-energy conditions. *Coast. Eng* 176, 104169. doi: 10.1016/j.coastaleng.2022.104169

Pan, Y., Zhou, Z. J., and Chen, Y. P. (2020). An analysis of the downward-flushing flow on the crest of a levee under combined wave and surge overtopping. *Coast. Eng.* 158, 103701. doi: 10.1016/j.coastaleng.2020.103701

Pedersen, M. F., and Borum, J. (2010). Nutrient control of estuarine mac-roalgae: growth strategy and the balance between nitrogen requirements and uptake. *Mar. Ecol-Prog Ser.* 1), 5–9. doi: 10.3354/meps161155

Riisgard, H. U., and Hoffmann, E. (2012). From fish to jellyfish in the eutrophicated limfjorden (Denmark). *Estuaries Coasts* 35, 701–713. doi: 10.1007/s12237-012-9480-4

Sheng, T. H., Sun, D. M., and Zhang, Y. (2016). Analysis of artificial island construction influences on individual flood erosion and deposition in estuary. *J. Waterway Harbor* 37 (1), 18–26.

Song, W., Wang, Z. L., Li, Y., and Zhang, X. L.. (2019). Tracking the original source of the green tides in the bohai Sea, China. *Estuarine Coast. Shelf Sci* 219, 354–362. doi: 10.1016/j.ecss.2019.02.036

Tang, W. J., Geng, H. X., Xi, Y. J., Zhang, Q. C., Tan, X. X., Yu, R.C., et al. (2022b). Mapping the resting cysts of dinoflagellate alexandrium catenella along the coast of qinhuangdao, China. *J. Oceanol Limnol* 40, 2312–2321. doi: 10.1007/s00343-022-2190-2

Tang, W. J., Lin, Z. R., Zhang, Q. C., Geng, H. X., Sun, H. X., Tang, X. X., et al. (2022a). An investigation on bloom dynamics of alexandrium catenella and a. pacificum and toxin accumulation in shellfish along the coast of qinhuangdao, China. *Mar. pollut. Bull* 183, 114058. doi: 10.1016/j.marpolbul.2022.114058

Valiela, I., McClelland, J., Hauxwell, J., Behr, P. J., Hersh, D., and Foreman, K. (1997). Macroalgal blooms in shallow estuaries: controls and ecophysiological and ecosystem consequences. *Limnol Oceanogr* 42, 1105–1118. doi: doi: 10.4319/lo.1997.42.5_part_2.1105

Yu, R. C., Zhang, Q. C., Liu, Y., Chen, Z. F., Geng, H. X., Dai, L., et al. (2021). The dinoflagellate alexandrium catenella producing only carbamate toxins may account for the seafood poisonings in qinhuangdao, China. *Harmful Algae* 103, 101980. doi: 10.1016/j.hal.2021.101980

Zhai, W. K., Xu, Z. Z., and Zhang, J. (2016). Analysis on characteristics of red tide disaster in hebei coastal waters. *Mar. Environ. Sci.* 35 (2), 243–251. doi: 10.13634/j.cnki.mes.2016.02.015

Zhang, W. Q., Han, H. B., and Qiu, L. M. (2022). Variations in nano- and pico-eukaryotic phytoplankton assemblages in the qinhuangdao green-tide area. *J. Oceanol Limnol* 40, 2446–2461. doi: 10.1007/s00343-022-2198-7

Zhang, W. L., Ma, X., Zhang, Y. F., Zhang, J. L., Zhao, S. L., Li, G. M., et al. (2020). An analysis of red tide characteristics in qinhuangdao coastal seawater. *Trans. Oceanol Limnol* 5, 48–55. doi: 10.13984/j.cnki.cn37-1141.2020.05.007

Zhang, Q. C., Yu, R. C., Zhao, J. Y., Kong, F. Z., Chen, Z. F., Niu, Z., et al. (2020). Distribution of aureococcus anophagefferens in relation to environmental factors and implications for brown tide seed sources in qinhuangdao coastal waters, China. *Harmful Algae* 109, 102015. doi: 10.1016/j.hal.2021.102105

Zhang, Z. H., Zhu, M. Y., Wang, Z. L., and Wang, J.. (2006). Monitoring and managing pollution load in bohai Sea, PR China. *Ocean Coast. Manage.* 49 (9), 706–716. doi: 10.1016/j.ocecoaman.2006.06.005

Zhao, Z. Y., and Kong, L. H. (2000). Environmental status quo and protection countermeasures in bohai marine areas. *Res. Environ. Sci.* 2), 23–27. doi: 10.13198/j.res.2000.02.26.zhaozhy.008

Zhou, Z. X., Kong, F. Z., Zhang, Q. C., Gao, Y., Koch, F., Gobler, C. J., et al. (2023). Brown tides linked to the unique nutrient profile in coastal waters of qinhuangdao, China. *Environ. Res.* 216, 114459. doi: 10.1016/j.envres.2022.114459